*10th International Conference on*
*Wood & Biofiber Plastic Composites*
~

# Transverse Elasticity of Cellulose Nanocrystals Via Atomic Force Microscopy

*Ryan Wagner, Arvind Raman, and Robert Moon*

## Abstract

The elastic properties of Cellulose Nanocrystals (CNCs) remain poorly characterized. Atomic force microscopy (AFM) methods were used to estimate the transverse elastic modulus ($E_t$) of individual, isolated CNCs derived from Tunicates. Understanding $E_t$ is important because it may lead to a better understanding of how CNCs behave in composite materials. Previous molecular modeling studies have shown the $E_t$ for CNCs to be between 11 to 57 GPa and were dependent on crystallographic orientation. This value is smaller than the axial modulus of 120 to 147 GPa. The main focus of this research is the interpretation of the AFM force curve data and the modeling implications when extracting $E_t$ using analytic continuum contact mechanics. Approximately thirty force curves were analyzed along the length of a single CNC. The distribution of $E_t$ has a mean of 9 GPa and a standard deviation of 2.6 GPa; however, by considering the uncertainty in the applied curve fitting procedure, the range of $E_t$ can be considered to be between 2 and 37 GPa. This distribution of modulus was considered to be a result of measuring a quantity near the noise floor of the AFM scanning procedure, rather than material property variation along the CNC.

**Wagner:**
Birck Nanotechnology Center, Purdue University, School of Mechanical Engineering, Purdue University, West Lafayette, Indiana

**Raman:**
Birck Nanotechnology Center, Purdue University, School of Mechanical Engineering, Purdue University, West Lafayette, Indiana

**Moon:**
Birck Nanotechnology Center, Purdue University, School of Materials Engineering, Purdue University, West Lafayette, Indiana, Forest Products Laboratory, U.S. Forest Service

## Introduction

Cellulose is the earth's most abundant biopolymer and is present in a wide variety of living species that use cellulose as a reinforcement material (trees, plants, tunicates—a group of abundant saclike filter feeding organism found in the oceans). In plants and trees, cellulose chains self-assemble into microcrystalline fibers, this base reinforcement unit provides high mechanical strength, high strength-to-weight ratio, and high toughness. Microcrystalline cellulose fibers are composed of crystalline and amorphous regions, and by selectively dissolving the amorphous regions with acid hydrolysis, the remaining crystalline regions can be liberated (Samir et al. 2005) and retain the natural cellulose I crystalline structure (Araki et al. 1998, Bondeson et al. 2006). These nanoscale cellulose crystals are called cellulose nanocrystals (CNCs).

Cellulose nanocrystals offer a unique "building block" on which a new biopolymer composites industry can be based (**Fig. 1**). The mechanical properties of CNCs are greater than other types of natural cellulosic materials (**Table 1**), and in some cases superior to other more traditional reinforcement materials (**Table 2**). Other advantages of CNCs are their high aspect ratio, low density (1.56 g/cm$^3$), and a reactive surface of –OH side groups that facilitates grafting chemical species to achieve different surface properties (surface functionalization). Surface functionalization allows the tailoring of CNC surface chemistry to facilitate self-assembly, controlled dispersion within a wide range of matrix polymers, and control of both the CNC-CNC and CNC-matrix bond strength.

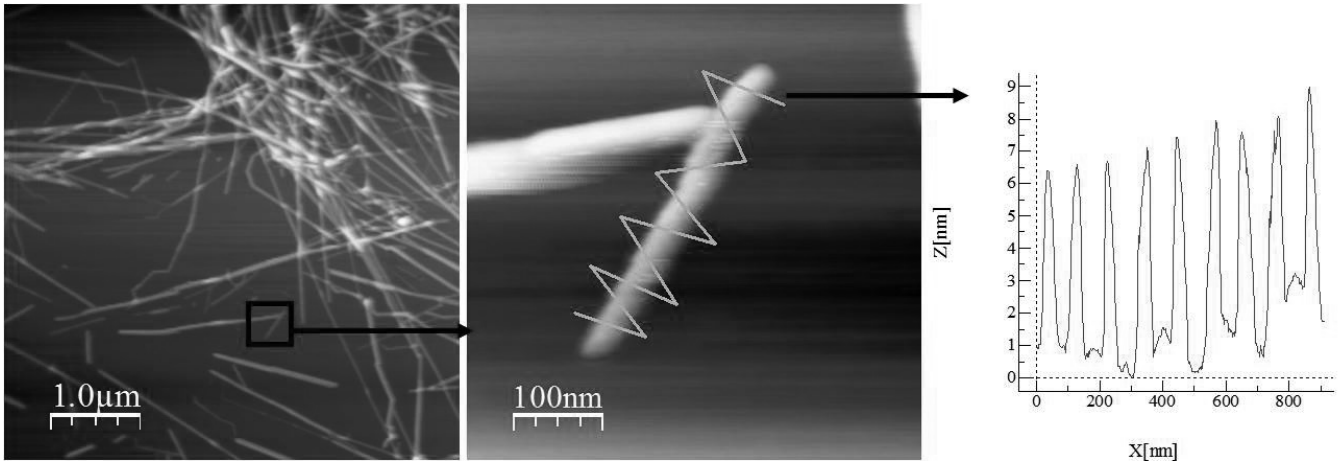


**Figure 1.** ~ *a) AFM topography map of CNCs deposited on mica, b) AFM topography map of an isolated CNC, c) height profile of the isolated CNC.*

**Table 1.** ~ *Properties of cellulose-based materials.*

| Material | Tensile strength | Elastic modulus | | Reference |
|---|---|---|---|---|
| | | $E_A$ † | $E_T$ ‡ | |
| | (GPa) | (GPa) | | |
| Cotton | 0.3–0.6 | 5.5–12.6 | – | Eichhorn et al. 2001 |
| Soft wood Kraft¶ | – | 17–20 | – | Neagu et al. 2006 |
| Loblolly pine | | | | |
| Earlywood | 0.3–0.7 | 14–18 | – | Mott et al. 2002 |
| Latewood | 0.4–1.4 | 19–27 | – | Mott et al. 2002 |
| Cellulose microfibrils | | | | |
| Ramie fibers | 0.8 | 27 | – | Ishikawa et al. 1997 |
| Flax and hemp | – | 25 ± 4 | – | Eichhorn and Young 2001 |
| Bacteria | – | 78 ± 17 | – | Guhados et al. 2005 |
| Cellulose I | | | | |
| Experimental | – | 120–135 | – | Matsuo et al. 1990 |
| Modeling | – | 124–155 | – | Tanaka and Iwata 2006 |
| | | | 11–57 | Jaswon et al. 1968, Tashiro and Kobayashi 1991 |
| | 7.5 | | 27 | Mark 1968 |
| Cellulose nanocrystals | – | 143 | – | Šturcová et al. 2005 |

†$E_A$ = Elastic modulus in axial direction.
‡$E_T$ = Elastic modulus in transverse direction.
¶Wood fiber mats tested in bending and tensile loading.

In spite of the great potential of CNCs as a functional nanoparticle for green polymer nanocomposite materials, a fundamental understanding of the CNC properties and their role in composite property enhancement is not available. The axial CNC properties have been considered of primary importance on composite properties, but the load-transfer from the matrix to the CNC through the CNC-matrix interface region dictates the composite mechanical properties (Eitan et al. 2006). Because of this, it is imperative to characterize the transverse CNC properties. Unfortunately, there is limited understanding of the intrinsic properties of CNCs. What is known is based on measurements of microcrystalline cellulose within its "native state" (i.e., within the wood or plant tissue prior to CNC extraction), and there is little consideration of property anisotropy resulting from the CNC crystalline structure. Without accurate knowledge of the intrinsic properties of CNCs, the advancement of CNC-based composites is seriously impeded.

The purpose of this study is to address this gap by developing the necessary protocols for using of atomic

**Table 2.** ~ *Properties of several reinforcement materials.*

| Material | Density | Tensile strength | Elastic modulus | | Reference |
|---|---|---|---|---|---|
| | | | $E_A$ † | $E_T$ ‡ | |
| | (g/cm³) | (GPa) | (GPa) | | |
| Fibers | | | | | |
| E-glass | 2.5 | 3.5 | 72 | – | Callister 1994 |
| Kevlar-49 | 1.4 | 3.5 | 124 | – | Callister 1994 |
| | | – | 130 | 2.5 | Kawabata et al. 1993 |
| Carbon | 1.8 | 1.5–5.5 | 150–500 | – | Callister 1994 |
| High carbon steel wire | 7.8 | 4.1 | 210 | – | Callister 1994 |
| Whiskers | | | | | |
| Graphite | 2.2 | 20 | 690 | – | Callister 1994 |
| Aluminum Oxide | 3.9 | 14–28 | 415–550 | – | Callister 1994 |
| Nanoparticles | | | | | |
| Clay platelets | – | – | 170 | – | Hussain et al. 2006 |
| MWCNTs¶ | – | 11–63 | 270–950 | – | Yu et al. 2000 |
| Boron whiskers | – | 2–8 | 250–360 | – | Ding and Himmel 2006 |
| Graphite platelets | – | – | 1000 | – | Hussain et al. 2006 |

†$E_A$ = Elastic modulus in axial direction.
‡$E_T$ = Elastic modulus in transverse direction.
¶MWCNTs: Multi-walled carbon nanotubes.

force microscopy (AFM) techniques to characterize CNCs' transverse mechanical properties.

## Background

### Atomic Force Microscopy

Atomic force microscopy is a diverse instrument that is capable of measuring nanometer-scale features on surfaces for a variety of materials (Binning and Quate 1986). A general AFM setup is shown in **Fig. 2**. Typically, an AFM works by bringing a sharp tip mounted on a mircocantilever into contact with a sample and monitoring the response of the cantilever with a laser photodiode system. The sample is mounted on a piezo-electric device providing precise displacement control in three dimensions. An AFM is capable of operating in several modes (tapping, contact, force displacement), and under many different environments (vacuum, vapor, fluid). Atomic force microscopy can measure many different surface properties, such as topography, elasticity, adhesion, thermal, and electrical (Butt et al. 2005).

Several AFM modes exist for measuring elastic properties of surfaces. Force displacement methods (Weisenhorn et al. 1989), force modulation microscopy (Maivaldt et al. 1991), and contact resonance AFM (Yamanka and Nakano 1998) are a few examples. In the current study, force displacement AFM is utilized because it is the simplest mode to implement and it allows for extensive model considerations to be made with respect to AFM tip-surface geometry. Its main disadvantage is that it is a static mode and cannot use a lock-in amplifier, thus having a higher noise floor.

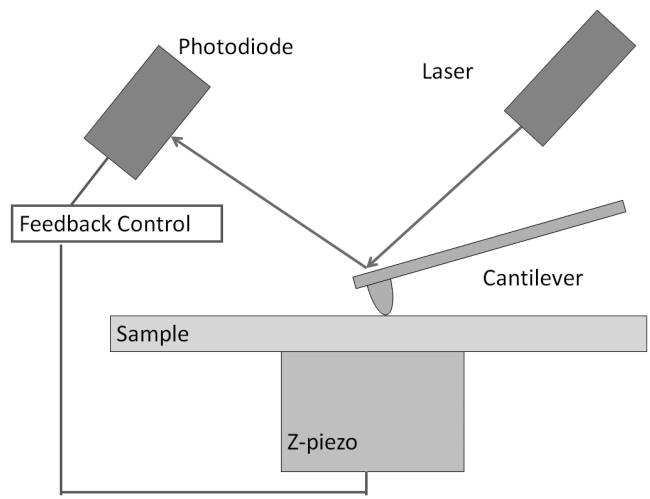


**Figure 2.** ~ *Typical AFM setup. Cantilever: 100–300 µm long, 20–40 µm wide, and 2–7 µm thick with a 10–30 µm long tip with a 2–10 nm shape tip at the end. Z-piezo: Used to move the sample. Laser-Photodiode System: Used to monitor the cantilever response. Feedback Control: Used to control the Z-piezo.*

In force-displacement mode, the force ($F$) is recorded as a function of the sample displacement ($Z$) (**Fig. 3a**). $F$ and $Z$ are calibrated in standard method (Butt et al. 2005). This process results in a force-displacement curve ($FZ$ curve). To relate the resulting elastic response within

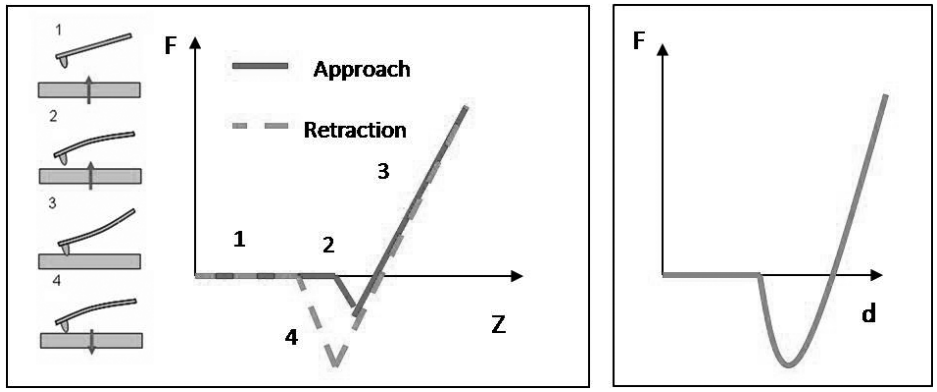


**Figure 3.** ~ *a) Force-displacement (*FZ*) curve: 1) Noncontact region—tip and sample do not interact; 2) jump to contact instability—attract force gradients cause the cantilever tip to snap into contact with each other; 3) elastic response—this region is used to exact elastic properties. The slope of the line represents the combined stiffness of the cantilever and sample. 4) Pull off force: This is the force required to with draw the tip from the sample; b) force-distance (*Fd*) curve: a model is fit to this curve to extract* $E_t$.

the *FZ* curve (Region 3) to the elastic properties of the sample the *FZ* curve must be converted into a force vs. tip-sample distance curve (*Fd* curve). This is accomplished by subtracting the cantilever defection (*D*) from the sample displacement (*Z*) (**Fig. 4**). This *Fd* curve describes the AFM tip indentation of the sample surface (**Fig. 3b**). The sample elastic modulus can be extracted from an *Fd* curve by fitting an appropriate material-mechanics model to the curve. This is a standard AFM method that has been used in many previous studies (Butt et al. 2005).

## Modeling

Several different models can be applied to force distance curves. These models include molecular dynamics simulation (MD), finite element modeling (FEM), and analytic continuum contact mechanics approaches. Molecular dynamics simulation solves the system response by considering the interaction between atoms and molecule. This is very powerful, but requires extensive knowledge about precise system characteristics as inputs, and is computationally expensive. Finite element modeling solves for the system response by dividing the system into many small elements and then considers a force balance on each element. It is not as computationally expensive as MD, but is based on continuum assumptions for system behavior that may break down at small scales. Typical analytic continuum contact mechanics work by solving a boundary value problem in a given domain for a given set of physical laws. Analytically based models require very little computational cost and can provide powerful insight into a material system. However, they also tend to be the least accurate in describing the actual system. This arises from the extensive assumptions often necessary to arrive at an analytic solution.

Hertzian contact mechanics is one example of an analytical contact mechanics model (Hertz 1896). Hertz contact is derived by assuming that contact is initialized at a single point (point contact) and that contact area evolves in an ellipse as the loading is increased. Hertz contact assumes that the material is isotropic, continuous,

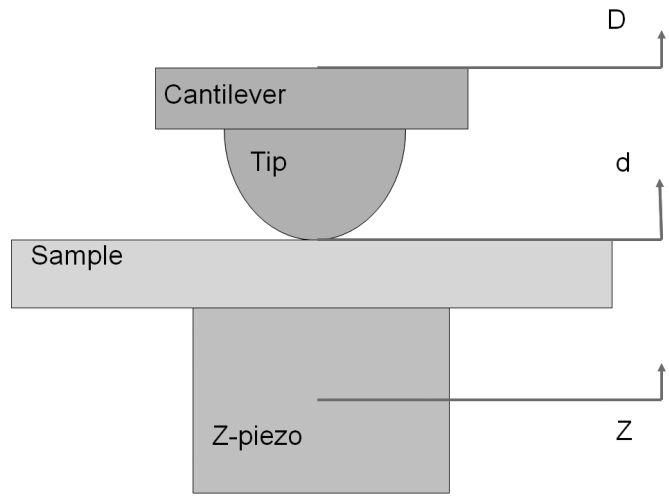


**Figure 4.** ~ *Coordinate system for force curve analysis:* D *is the cantilever displacement,* d *is the tip sample deformation, and* Z *is the sample piezo (Z-piezo) motion.*

piecewise smooth, semi-infinite, frictionless, and adhesive forces are not present. Despite its simplicity Hertz contact is still useful and often appears in AFM literature because of its ease of implementation.

## Experimental Procedure

Tunicate CNC samples were provided by Professor Christoph Weder of Case Western Reserve University. The preparation of these crystals is described elsewhere (Berg et al. 2007). Tunicate CNCs are used in this study because they exhibit more uniform shape compared to other CNC sources; furthermore, tunicate whiskers are slightly larger than other CNC sources and tend to agglomerate less. These CNC whiskers have lengths that range from 500 to 10,000 nm and diameters that vary from 5 to 20 nm (**Fig. 1**). This corresponds to an aspect ratio (L/D) of 25 to 1000. For AFM work a 0.1 mg/mL aqueous CNC solution was deposited on freshly cleaved grade V1 mica and allowed to sit in a nitrogen atmosphere overnight.

A Nanotec Electronica AFM and Dulcinea controller (Madrid, Spain) was used to measure force-displacement

curves on a single isolated CNC. Measurements were done in dry nitrogen (RH ~ 0.1%) to minimize meniscus effects. AppNano FORT force modulation cantilevers (AppNano.com) with a nominal spring constant of 3 N/m were used for imaging. Each cantilever was calibrated via Sader's method to determine the actual stiffness (Sader et al. 1999). Image processing was done in the WSxM (version 4.0) software (Horcas et al. 2007).

Force volume (FV) mode in the WSxM software was used to acquire simultaneous topography and force displacement data. Force volume mode is similar to standard force displacement AFM, except that the feedback is turned on between the forward and backward curves to acquire surface location. Surface location is defined as a set amount of cantilever defection (set point). Force volume mode creates a map of topography and force displacement curves over a specified area. 128 × 128 pixel maps were acquired on the CNC/mica surface, typically over an area about 300 × 300 nm. The set point for the topography image was approximately 40 nN. Each force displacement curve consists of about 125 data points, has a *Z* ramp range of about 80 nm, and was acquired at a rate of about 30 Hz per *FZ* curve. By creating a map of the surface *FZ* curves can be analyzed at any location on a CNC.

## Analysis Technique for Elasticity Extraction

Four steps were used for extraction of transverse elastic modulus ($E_t$) of CNCs from AFM measurements. First, *FZ* curves must be measured on the CNC. Second, the *FZ* curve must be converted into an *Fd* curve. Third, an appropriate model must be fit to the *Fd* data. Fourth, $E_t$ must be extracted from the model.

To convert an *FZ* curve into an *Fd* curve the distance, *d* corresponding to a given sample displacement, *Z* is given by:

$$d = Z - D \qquad [1]$$

where *D* is the cantilever deflection corresponding to a given sample displacement (**Fig. 4**).

Next, a model is fit to the *Fd* curve. For a preliminary analysis the Hertz model for a sphere contacting a cylinder was employed (Boresi 1978). The sphere approximates the AFM-tip and the cylinder approximates the CNC. The Hertz solution predicts a force distance relationship of the form:

$$F = Cd^{3/2} \qquad [2]$$

where *C* is a constant related to surface geometry and material properties. Specifically:

$$C = \frac{2\pi\left[E(k_p)\right]^{1/2}}{3k\left[K(k_p)\right]^{3/2}(A+B)^{3/2}\Delta} \qquad [3]$$

$$A \equiv \frac{1}{2R_s},\ B \equiv \frac{1}{2}\left(\frac{1}{R_s}+\frac{1}{R_c}\right) \qquad [4, 5]$$

$$E(k_p) \equiv \int_0^{\pi/2}\sqrt{1-k_p^2\sin^2(\theta)}\,d\theta,\ K(k_p) \equiv \int_0^{\pi/2}\frac{d\theta}{\sqrt{1-k_p^2\sin^2(\theta)}} \qquad [6, 7]$$

$$\Delta \equiv \frac{1}{A+B}\left(\frac{1-v_s^2}{E_s}+\frac{1-v_c^2}{E_c}\right) \qquad [8]$$

where $R_i$ is the radius, $E_i$ is the Young's modulus of the material, $\nu_i$ is the Poisson's ratio of the material, subscript *S* represents the sphere, and subscript *C* represents the cylinder. The constant *k* is the ratio of the major and minor axis of the contact ellipse. Where *k* and $k_p$ are found by numerically solving:

$$\frac{B}{A} = \frac{1/(1-k_p^2)*E(k_p)-K(k_p)}{K(k_p)-E(k_p)},\ k_p \equiv \sqrt{1-k^2} \qquad [9,10]$$

Several AFM studies have used the similar models (Palaci et al. 2005, Zhao et al. 2008). Based on **Eq. [2]**:

$$F = k_L a(d_p + b)^{3/2} \qquad [11]$$

is an appropriate functional form to fit to the *Fd* data. In **Eq. [11]**, $k_L$ is the cantilever stiffness, *a* is the elasticity fitting parameter related to $E_t$, *b* is a fitting parameter that corrects for the fact that the zero surface displacement is arbitrarily defined (surface fitting parameter), and $d_p$ is the distance prior to this offset correction. In terms of **Eq. [3]**:

$$C = k_L a \qquad [12]$$

thus *a* can be related to $E_t$ by **Eqs. [3–10]**. **Equation [11]** is fitted to the *Fd* data with a nonlinear least squares fitting procedure.

## Results and Discussion

*FZ* data collected on an isolated tunicate CNC are shown in **Fig. 5**. A segment of an isolated 5 nm diameter CNC is analyzed (**Fig. 5a**). The map consists of 128 × 128 *FZ* curves. 32 *FZ* approach curves were extracted along the apex of the crystal (~60 nm length segment) because that is where the contact geometry is closest to the modeling assumptions (**Fig. 5b**).

The 32 converted *Fd* data sets and corresponding curve fits from **Eq. [11]** are shown in **Fig. 6**. For each of these curve fits, the $R^2$ value, the 95% confidence interval (CI), and the value of the *a* fitting parameter are shown in **Fig. 7** and **8** respectively. The $R^2$ value represents how well the model function fits the data. $R^2$ values near one indicate good agreement with the model function and $R^2$ values far from one indicate poor agreement. The $R^2$ values in this study fall in an intermediate region. The 95% CIs are the range in which the algorithm is 95% confident the fitting parameter is within. Understanding this range is important for understanding the uncertainty in the final reported value of $E_t$. Ultimately, the main output from this process is the distribution of the fitting

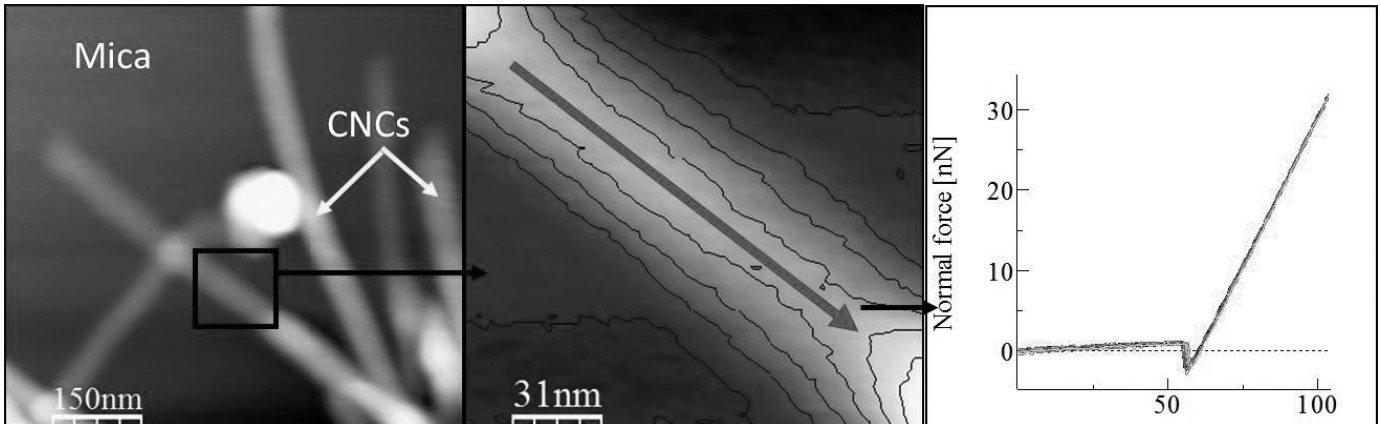


**Figure 5.** ~ *The Tunicate CNC tested in this study. a) Topography of CNCs on mica, b) AFM topography image acquired with force displacement data. CNC diameter is approximately 5 nm (after removing the influence of AFM-tip dilation effects, which makes the CNC appear to be 50 nm wide), c) force-displacement curves where extracted from 32 points along the apex of the CNC (blue line).*

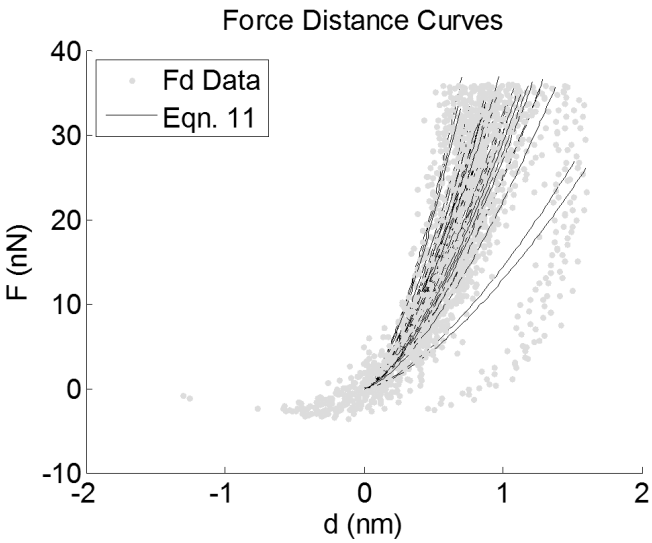


**Figure 6.** ~ *Converted AFM force distance data and overlaying Hertzian curve fits for the 32* FZ *curves in* **Fig. 5**. *Blue dots represent processed data and black curves represent curve fits. 32* Fd *curves are considered, but there are two apparent outlier curves that should be noted.*

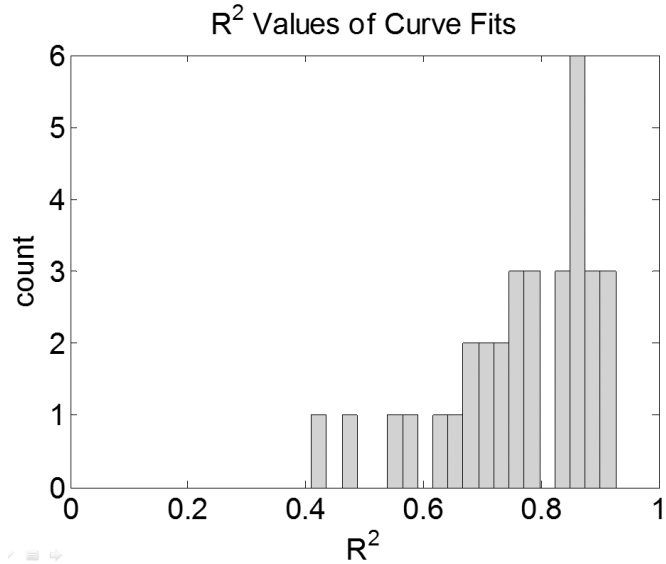


**Figure 7.** ~ $R^2$ *values of the* **Eq. [11]** *curve fits of the* Fd *data shown in* **Fig. 6**. $R^2$ *values near one indicate good agreement between the curve fits and experimental data. The lowest two* $R^2$ *values are for the two apparent outlier curves.*

parameter $a$. The mean value of $a$ is 30 $nm^{-1/2}$ and the standard deviation of $a$ is 9 $nm^{-1/2}$. Note that two curves, which correspond to curve fit numbers 17 and 18, appear to be outliers. By removing them, the lowest two $R^2$ values are removed and the mean value of $a$ becomes 32 $nm^{-1/2}$ and the standard deviation of $a$ is 8 $nm^{-1/2}$.

The large variations of these parameters can result from several factors, such as variations in contact geometry, large changes in materials properties within the CNC, and the measured quantities being near the noise floor of the AFM system. Since the tunicate CNCs are very uniform in height and *FZ* curves are obtained from the CNC apex (**Fig. 5b**), the main cause of variations in contact geometry would be AFM-tip shape changing from one *FZ* curve to the next. This is considered unlikely as this effect would result in systematic changes in topography from image to image and this was not observed. Nor are the large distributions likely to be from changes in material properties within the crystal. Tunicate CNCs have highly uniform diameters along the length and likely have uniform material properties as well. Additionally, the region of the tunicate CNC from which measurements were analyzed were along a straight region of the whisker far removed from the end regions of the crystal, thus minimizing the likelihood of defects being introduced into the structure (**Fig. 5**). The most likely source of the variations is considered to result from the noise in the AFM measurements, which can come from many sources. In this study it is likely that hysteresis of the Z-piezo and thermal, electrical, and mechanical noise in

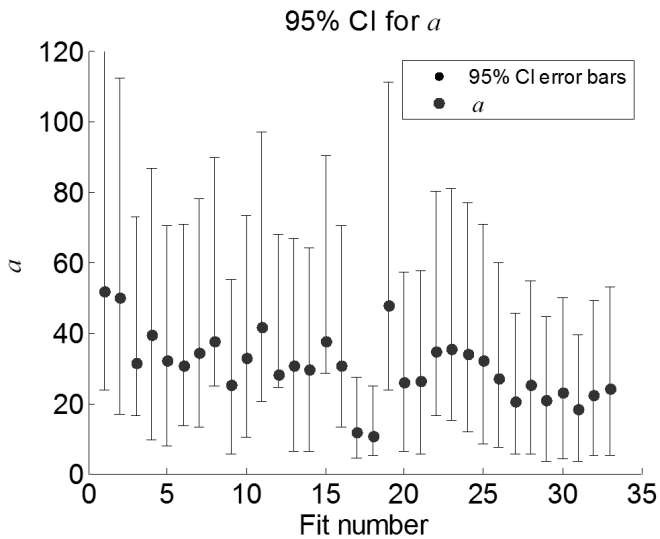


**Figure 8.** ~ *The 95% confidence intervals (CIs) and values for the fitting parameter* a *extracted from the curve fits for each* Fd *data set. The 32 data sets represent the 32 locations along the CNC (in* **Fig. 5b***) in which the* FZ *curves were analyzed for this study.*

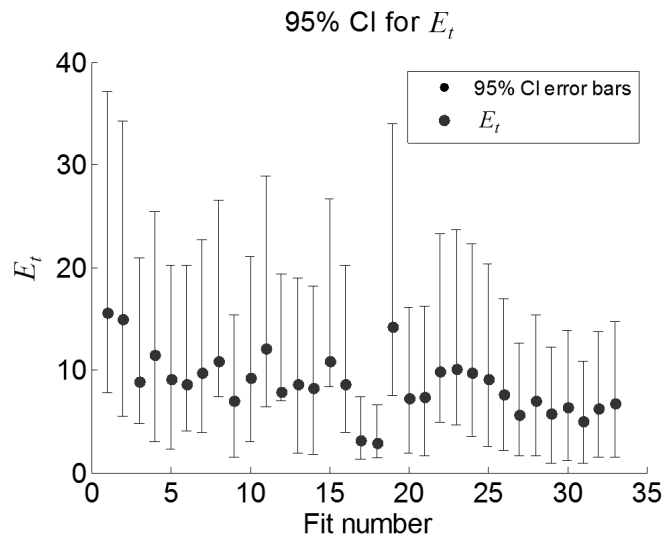


***Figure 9.*** ~ *The 95% CIs for the transverse modulus,* $E_t$, *calculated from the distributions of* a *given in* **Fig. 8**.

the cantilever response are the dominant sources. Since the distance measurement is the difference of these quantities, noise from both sources contributes the scatter of $d$. This combined noise is significant when compared to the maximum magnitude of $d$, which is about 5 angstroms. Therefore, it is likely that the measured quantity being near the noise floor of the AFM measurement system is responsible for the large scatter in the data and thus the large range of outputs from the fitting algorithm. This issue can be addressed by lowering the noise floor via improvements in the measurement system or by analyzing a large number of *FZ* curves.

The parameter $a$ can be related to $E_t$ by **Eqs. [3–10]** with parameter values of: $E_{tip}$ = 100 GPa, $\nu_{tip}$ = 0.3, $\nu_{cnc}$ = 0.3, $R_{tip}$ = 20 nm, $R_{cnc}$ = 5 nm. **Figure 9** shows the calculated $E_t$ and the 95% CI for each curve fit. The distribution of $E_t$ on this isolated CNC has a mean of 9 GPa and a standard deviation of 2.6 GPa (excluding the two apparent outlier curves fit 17 and 18). If the 95% CI of the fitting parameter $a$ is considered, then the 95% CI range of $E_t$ is 2 to 37 GPa. This suggests a much greater range in the measured value of $E_t$. The predicted value of $E_t$ is in agreement with previous molecular dynamics modeling studies (Jaswon et al. 1968, Mark 1968, Tashiro and Kobayashi 1991). As indicated earlier, this large range in transverse modulus is not likely to result from large changes in properties along CNC length, but rather from the measurement being close to the noise floor of the AFM measurement system used in the current study.

Additionally, it should be noted that an isotropic model is being used to extract an anisotropic material property; thus, the significant output is not so much the prediction of $E_t$ but the demonstration of the ability to map out material property measurements with nanometer-scale resolution within a statistical framework on a surface with significant geometric features. This procedure could potentially be used to analyze a very large number of *FZ* curves and study the variability of elastic properties within a single CNC and between CNCs with an extensive uncertainty analysis. In the future more sophisticated material models will be considered and the analysis will be performed for a large number of CNCs.

## Conclusion

An analysis of AFM force-displacement curves (*FZ* curves) on an isolated tunicate-derived CNC was performed. The *FZ* curves were converted into force-distance curves (*Fd* curves) and fit with a Hertz contact model to extract $E_t$. One isolated CNC was analyzed and $E_t$ was found to have a distribution with a mean value of 9 GPa and a 2.6 GPa standard deviation. By incorporating uncertainty in the curve fit parameter $a$ (used to calculated $E_t$) it expands the range of possible $E_t$: 2 to 37 GPa. The wide distribution of this estimated modulus was not likely a result of material property variation within the CNC, but rather a result of measuring a quantity near the noise floor of the AFM scanning procedure. When considering this number it is important to remember the modeling limitations in its derivation, specifically, that an isotropic model was used to extract an anisotropic property. Nevertheless, this technique can provide insight into the distribution of transverse mechanical properties of CNCs.

## Acknowledgments

The authors would like to thank U.S. Forest Services, Purdue University Graduate School, and Discovery Park at Purdue University for funding this project. We would like to thank Professor Ron Reifenberger from Purdue University Department of Physics for his helpful

experimental advice and we are grateful for Professor Christoph Weder's research group from Case Western University for providing the tunicate samples.

## Literature Cited

Araki, J., M. Wada, S. Kuga, and T. Okano. 1998. Flow properties of microcrystalline cellulose suspension prepared by acid treatment of native cellulose. Colloid Surface A. 142:75–82.

Berg, O., J.R. Capadona, and C. Weder. 2007. Preparation of homogenous dispersions of tunicate cellulose whiskers in organic solvents. Biomacromolecules. 8:1353–1357.

Binning, G., and C.F. Quate. 1986. Atomic Force Microscope. Phys. Rev. Lett. 56(9):930–933.

Bondeson, D., A. Mathew, and K. Oksman. 2006. Optimization of the isolation of nanocrystals from microcrystalline cellulose by acid hydrolysis. Cellulose. 13:171–180.

Boresi, A.P. 1978. Advanced Mechanics of Materials, 3rd Edition. John Wiley & Sons, Inc., New York.

Butt, H., B. Cappella, and M. Kappl. 2005. Force measurements with the atomic force microscope: technique, interpretation and applications. Surf. Sci. Rep. 59:1–152.

Callister, W. 1994. Composites Materials Science and Engineering: An Introduction. John Wiley & Sons, Inc., New York.

Ding, S.Y., and M.E. Himmel. 2006. The maize primary cell wall microfibril: A new model derived from direct visualization. J. Agric. Food Chem. 54:597–606.

Eichhorn, S.J., C.A. Baillie, N. Zafeiropoulos, L.Y. Mwaikambo, M.P. Ansell, A. Dufresne, K.M. Entwistle, P.J. Herrera-Franco, G.C. Escamilla, L. Groom, M. Hughes, C. Hill, T.G. Rials, and P.M. Wild. 2001. Review: Current international research into cellulosic fibres and composites. J. Mat. Sci. 36:2107–2131.

Eichhorn, S.J., and R.J. Young. 2001b. The Young's modulus of a microcrystalline cellulose. Cellulose. 8:197–207.

Eitan A., F.T. Fisher, R. Andrews, L.C. Brinson, and L.S. Schadler. 2006. Reinforcement mechanisms in MWCNT-filled polycarbonate. Compos. Sci. Technol. 66:1162–1173.

Guhados G., W. Wan, and J.L. Hutter. 2005. Measurement of the elastic modulus of single bacterial cellulose fibers using atomic force microscopy. Langmuir. 21: 6642–6646.

Hertz, H. 1896. Miscellaneous papers. Macmillan, London, UK. pp. 146–161.

Horcas, I., R. Fernandez, J.M. Gomez-Rodriguez, J. Colchero, J. Gomez-Herrero, and A. M. Baro. 2007. WSXM: A software for scanning probe microscopy and a tool for nanotechnolgy. Rev. Sci. Instrum. 78:013705.

Hussain, F., M. Hojjati, M. Okamoto, and R.E. Gorga. 2006. Polymer-matrix nanocomposites, processing, manufacturing, and application: An overview. Compos. Mater. 40:1511–1575.

Ishikawa, A., T. Okano, and J. Sugiyama. 1997. Fine structure and tensile properties of ramie fibers in the crystalline form of cellulose I, II, III and IV. Polymer 38(2):463–468.

Jaswon, A., P.P. Gillis, and R.E. Mark. 1968. The elastic constants of crystalline native cellulose. The Royal Society 306:389–412.

Kawabata, S., M. Sera, T. Kotani, K. Katsuma, M. Niwa, and C. Xiaoxin. 1993. Anisotropic mechanical properties of advanced high performance fibers obtained by a single fiber testing system. In 9th International Conference on Composite Materials. pp. 671– 677.

Maivaldt, P., H.J. Butt, A.C. Gould, C.B. Prater, B. Drakei, J.A. Guriey, B. Eiingsi, and P. Hansma. 1991. Using force modulation to image surface elasticities with the atomic force microscope. Nanotechnology 2:103–106.

Mark, R.E. 1968. Cell Wall Mechanics of Tracheids, Yale University Press, New Haven, NJ.

Matsuo, M., C. Sawatari, Y. Iwai, and F. Ozaki. 1990. Effects of orientation distribution and crystallinity on the measurement by X-ray diffraction of the crystal lattice moduli of cellulose I and II. Macromolecules 23:3266–3275.

Mott, L., L. Groom, and S. Shaler. 2002. Mechanical properties of individual southern pine fibers. Part II. Comparison of earlywood and latewood fibers with respect to tree height and juvenility. Wood Fib. Sci. 34(2):221–237.

Neagu, R.C., E.K. Gamstedt, and M. Lindström. 2006. Characterization methods for elastic properties of wood fibers from mats for composite materials. Wood Fib. Sci. 38:95–111.

Palaci, I., S. Fedrigo, H. Brune, C. Klinke, M. Chen, and E. Riedo. 2005. Radial elasticity of multiwalled carbon nanotubes. Phys. Rev. Lett. 94:175502.

Sader, J.E., J.W. Chon, and P. Mulyaney. 1999. Calibration of rectangular atomic force microscope cantilevers. Rev. Sci. Instrum. 70(10):3967–3969.

Samir M.A., F. Alloin, and A. Dufresne. 2005. Review of recent research into cellulosic whiskers, their properties and their application in nanocomposite field. Biomacromolecules 6:612–626.

Sturcova, A., G.R. Davies, and S.J. Eichhorn. 2005. The elastic modulus and stress-transfer properties of tunicate cellulose whiskers. Biomacromolecules 6:1055–1061.

Weisenhorn, A.L., P.K. Hansma, T.R. Albrecht, and C.F. Quate. 1989. Force in atomic force microscopy in air and water. Appl. Phys. Lett. 54(26):2651–2653.

Tanaka, F., and T. Iwata. 2006. Estimation of the elastic modulus of cellulose crystal by molecular mechanics simulation. Cellulose 13:509–517.

Tashiro, K., and M. Kobayashi. 1991. Theoretical evaluation of three-dimensional elastic constants of native and regenerated celluloses: role of hydrogen bonds. Polymer 32:1516–1526.

Yamanka, K., and S. Nakano. 1998. Quantitative elasticity evaluation by contact resonance in and atomic force microscope. Appl. Phys. A. 66:S313–S317.

Yu, M.F., O. Lourie, M. Dyer, K. Moloni, T. Kelly, and R. Ruoff. 2000. Strength and breaking mechanism of multiwalled carbon nanotubes under tensile load. Science 287:637–640.

Zhao, Y., G. Zhibin, and J. Fang. 2008. Elastic modulus of viral nanotubes. Phys. Rev. E. 78:031914.

Tenth International Conference on Wood & Biofiber Plastic Composites and Cellulose Nanocomposites Sysmposium, May 11-13, Madison, WI. Madison, WI : Forest Products Society, c2010. ISBN 978-1-892529-55-8.